EXCEPTIONAL CASE REPORT

blood advances

Novel *SF3B1* in-frame deletions result in aberrant RNA splicing in CLL patients

Anant A. Agrawal,[1,*] Michael Seiler,[1,*] Lindsey T. Brinton,[2] Rose Mantel,[2] Rosa Lapalombella,[2] Jennifer A. Woyach,[2] Amy J. Johnson,[2] Ping Zhu,[1] Markus Warmuth,[1] Lihua Yu,[1] John C. Byrd,[2] Peter G. Smith,[1] James S. Blachly,[2,†] and Silvia Buonamici[1,†]

[1]H3 Biomedicine, Inc., Cambridge, MA; and [2]Ohio State University Comprehensive Cancer Center, Columbus, OH

Key Points

- We identify and characterize novel *SF3B1* in-frame deletions in chronic lymphocytic leukemia.
- These deletions are functionally similar to well-known *SF3B1* hotspot mutations and are sensitive to splicing modulation.

Introduction

Hematologic neoplasms including myelodysplastic syndromes (MDSs), chronic lymphocytic leukemia (CLL), chronic myelomonocytic leukemia, and acute myeloid leukemia have recently been reported to contain heterozygous hotspot mutations in splicing factor genes involved with 3′ splice site (ss) recognition (*SF3B1*, *U2AF1*, *SRSF2*, and *ZRSR2*).[1-4] In contrast to other disorders, CLL is unique in that only *SF3B1* is recurrently mutated.[2] The spliceosome machinery directs the removal of introns from transcripts followed by ligation of coding exons during RNA splicing.[5] The recently solved eukaryotic spliceosome structures indicate that *SF3B1* HEAT domains interact with the branch site and polypyrimidine (Py) tract.[6-8] Although the majority of *SF3B1* hotspot mutations are located in the Py tract interacting region, the reason for inducing aberrant 3′ ss selection through reduced branch site fidelity remains unclear.[9-13]

The unique signature of aberrant 3′ ss junction usage by SF3B1 mutations suggests that these events can be used as biomarkers to discover additional genomic alterations that lead to similar splicing defects. To this end, we analyzed RNA sequencing (RNA-seq) from 215 CLL patients. We discovered 3 patients carrying 2 novel *SF3B1* in-frame deletions, and we demonstrate that these deletions induce aberrant 3′ ss selection through use of an alternative branch site, similar to SF3B1 p.K700E. In addition, patient samples carrying these deletions showed sensitivity to the splicing modulator E7107. Functionally, these novel deletions act similarly to other well-known *SF3B1* hotspot mutations suggesting patients carrying these lesions are candidates for treatment with SF3B1 modulators.

Case description

Recurrent mutations in RNA splicing factors *SF3B1*, *U2AF1*, and *SRSF2* have been reported in hematologic cancers including MDSs and CLL. However, CLL is unique considering that only *SF3B1* is found to be recurrently mutated and associated with aberrant splicing. To investigate whether other genomic aberrations cause similar splicing defects, we clustered RNA-seq data based on an alternative 3′ ss pattern previously identified in *SF3B1*-mutant CLL patients. Among 215 samples, we identified 37 (17%) with alternative 3′ ss usage, the majority of which harbored known *SF3B1* hotspot mutations. Intriguingly, 3 patient samples carried previously unreported in-frame deletions in *SF3B1* around K700, the most frequent mutation hot spot. To study the functional effects of these deletions, we used various minigenes demonstrating that recognition of canonical 3′ ss and alternative branch site are required for aberrant splicing, as observed for *SF3B1* p.K700E. The common mechanism of action of these deletions and substitutions result in similar sensitivity of primary cells toward an SF3B1 splicing modulator. These data demonstrate a novel genomic aberration in *SF3B1* that induces aberrant splicing and suggest *SF3B1* in-frame deletions will confer sensitivity to splicing modulators.

Submitted 22 March 2017; accepted 8 May 2017. DOI 10.1182/bloodadvances.2017007062.

*A.A.A. and M.S. contributed equally to this study.

†J.S.B. and S.B. are joint senior authors.

The RNA-sequencing data analyzed and presented in this article have been deposited in the Gene Expression Omnibus database (accession number GSE95352). The DNA-sequencing data analyzed and presented in this article have been deposited in the Sequence Read Archive (accession number SRP100874).

The full-text version of this article contains a data supplement.

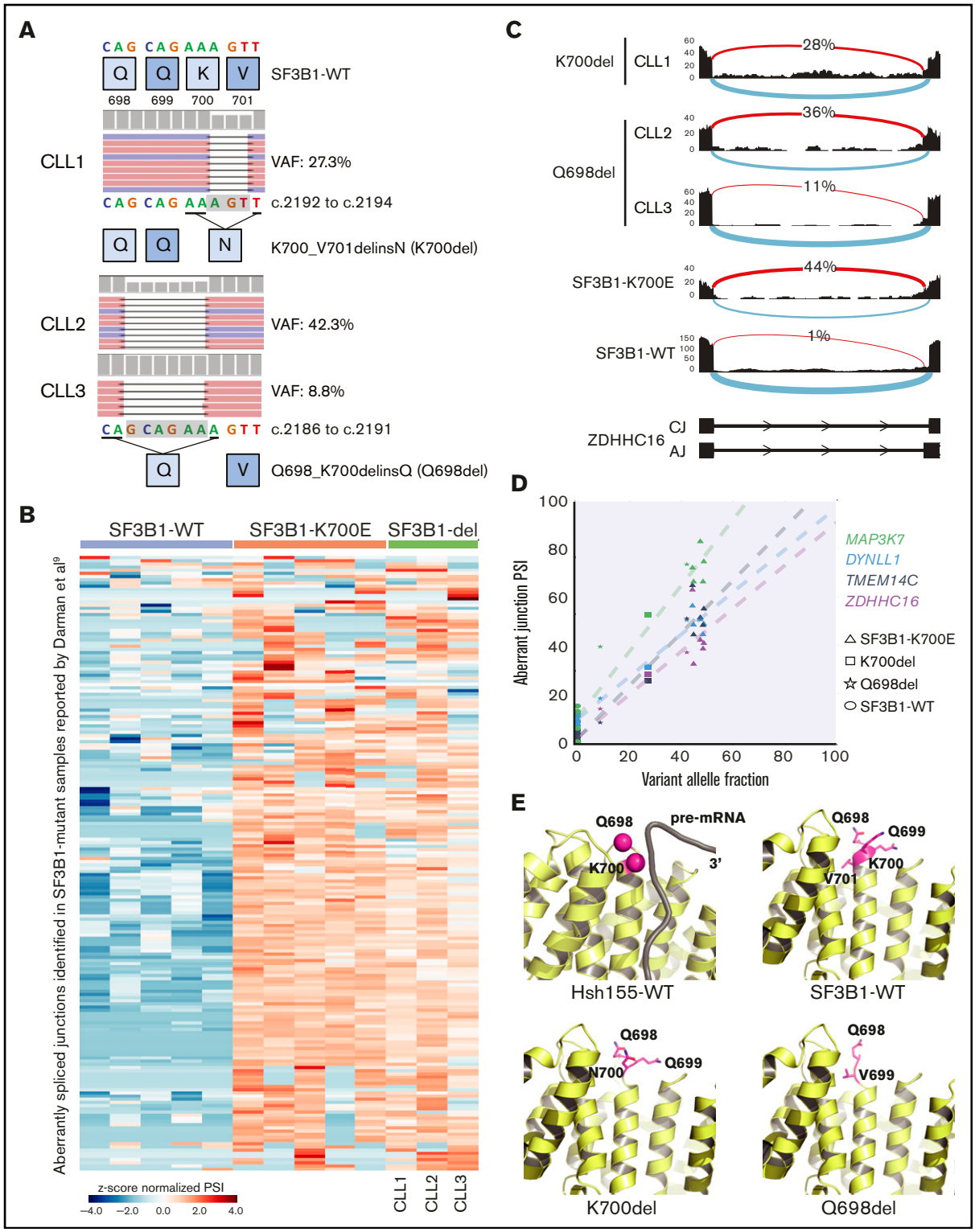

Figure 1. Novel *SF3B1* in-frame deletions found in CLL patients result in aberrant splicing. (A) DNA sequencing reads from 3 CLL patients are aligned to show *SF3B1* in-frame deletions: CLL1, p.K700_V701delinsN (p.K700del); CLL2 and CLL3, p.Q698_K700delinsQ (p.Q698del). The schematic below shows the 3 nt and 6 nt deletions resulting in replacement of K700 and V701 with N and of Q698, Q699, and K700 with Q, respectively. The deletion is highlighted in a gray box. (B) Heat map representing *z* score normalized percent spliced in (PSI) of aberrant junctions previously identified in *SF3B1*-mutant CLL patient samples (n = 194). Sample columns are grouped into *SF3B1* variants: *SF3B1* wild type (WT; n = 5), *SF3B1* p.K700E (n = 5), and *SF3B1* deletion mutants (n = 3). (C) Sashimi plot showing aberrant 3′ ss usage (red) with respect to canonical splicing (light blue) of *ZDHHC16* exons 9 to 10 in different CLL patient samples: K700del (CLL1), Q698del (CLL2 and CLL3), *SF3B1* p.K700E, and *SF3B1* WT. The aberrant junction PSI is given as a percentage in each condition. For *SF3B1* p.K700E and *SF3B1* WT, the average read density and PSI is plotted (n = 5, each). (D) Four *SF3B1* hotspot-specific aberrant ss's show

Methods

RNA-seq from 215 CLL patients was analyzed to discover if any novel genomic abnormality was able to induce *SF3B1*-mutant-like aberrant splicing. Genomic abnormalities in 3 aberrant splicing cases were identified as *SF3B1* in-frame deletions and confirmed in DNA by targeted resequencing. Analysis of RNA splicing was carried out as described previously.[9] Expression of hemagglutinin (HA)-tagged mxSF3B1 deletion complementary DNAs transfected into HEK293FT cells was confirmed by quantitative polymerase chain reaction (qPCR) and immunoblotting. Aberrant splicing was validated using *ZDHHC16* minigenes and viability effect of E7107 in CLL primary cells was assessed by 3-(4,5 dimethylthiazol-2-yl)-5-(3-carboxymethoxyphenyl-2-(4-sulfophenyl)-2H-tetrazolium (MTS) assay. Methods in detail can be found in the supplemental Data.

Results and discussion

To investigate if genomic abnormalities in addition to known hotspot mutations in *SF3B1* led to *SF3B1*-mutant-like splicing aberrations in CLL patients, we clustered RNA-seq data from 215 samples based on previously identified *SF3B1*-mutant specific alternative 3′ ss in CLL (n = 194).[9] Of 215 samples, we identified 37 (17%) with alternative 3′ ss usage, 34 of which harbored known *SF3B1* hotspot mutations including p.K700E. Interestingly, 3 patient samples carried previously unreported in-frame deletions in *SF3B1*: 1 patient had a 3 nucleotide (nt) deletion resulting in replacement of K700 and V701 with N (p.K700_V701delinsN, "p.K700del") and 2 patients had 6 nt deletion resulting in replacement of Q698, Q699, and K700 with Q (p.Q698_K700delinsQ; "p.Q698del") (Figure 1A). The *SF3B1* deletion variant allele fraction (VAF) ranged from 8.8% to 42.2%, confirmed through RNA-seq and DNA sequencing. All 3 patients had poor prognostic features including unmutated *IGHV* status and high-risk cytogenetics (supplemental Table 1). Notably, a different *SF3B1* in-frame deletion (p.Q699_K700del) has also been reported both in MDS[14,15] and 2 cases of CLL[16,17]; however, its function remains uncharacterized.

In order to confirm that all the splicing aberrations found in mutant SF3B1 were observed in the novel deletion mutants, we selected 5 CLL patient samples with high VAF *SF3B1* p.K700E and compared the expression of various aberrant splicing markers (Figure 1B), including the aberrant 3′ ss in intron 9 of *ZDHHC16* (Figure 1C). Interestingly, all 3 samples with *SF3B1* in-frame deletions showed all the aberrant 3′ ss selections observed in the *SF3B1*-mutant patient samples, and we observed a direct correlation between VAF and 4 selected aberrant splicing biomarkers (Figure 1D).[9,18,19] Collectively, this analysis strongly suggested that *SF3B1* deletions acquire a neomorphic function similar to p.K700E. Structural modeling of the p.K700del and p.Q698del mutations in SF3B1 indicated they were located at the edge of α-helix of HEAT repeat domain 6, a region critical for pre-mRNA interaction (Figure 1E, top panel).[6,7] Deletion of key residues in the loop region could eliminate charged side-chain interaction of lysine with pre-mRNA or restrain conformational change in SF3B1 superhelical HEAT repeats affecting RNA/protein interactions (Figure 1E, bottom panel).

After confirming the expression of these *SF3B1* in-frame deletions by qPCR and their incorporation in the core SF3b complex by coimmunoprecipitation (Figure 2A-B), we used *ZDHHC16* minigenes to study the mechanism of induction of aberrant splicing.[9] As expected, when Exon9-Intron9-Exon10 (E9-I9-E10) minigene was cotransfected with WT, only canonical splicing was observed (Figure 2C, lane 3), whereas in cells expressing p.K700del and p.Q698del and the hotspot mutations (p.K700E and p.K700N), both canonical and aberrant splicing were detected (lanes 4-7). Previously, through modifications in canonical 3′ ss, cryptic 3′ ss, branch sites, and Py tracts, we demonstrated that recognition of both canonical 3′ ss and alternate branch site are required for aberrant splicing of *ZDHHC16* by SF3B1 hotspot mutants.[9] To address the dependence of cryptic 3′ ss selection by the in-frame deletions on canonical 3′ ss, we altered the nucleotide base upstream of the AG dinucleotide (canonical, −3T>G; aberrant, −24C>G) that is critical for U2AF1 interaction.[20] When −3T>G minigene was cotransfected with any of the constructs splicing was observed within exon 10 (Figure 2C, lanes 8-12). Whereas, when −24C>G minigene was used, only canonical splicing was observed in all cases (lanes 13-17), suggesting that the −3 position relative to cryptic AG is also important for its recognition during the second step of splicing. Further to test branch site utilization, we used *ZDHHC16* minigenes with mutated branch sites (WT, −30A>G; mutant, −33 to −35 AAA>GGG). When −30A>G minigene was cotransfected with WT, splicing was observed within exon 10 (Figure 2D, lane 1), but when cotransfected with p.K700E or in-frame deletions, only aberrant splicing was observed (Figure 2D, lanes 2-5). When −33 to −35 AAA>GGG minigene was cotransfected with p.K700E or in-frame deletions, only canonical splicing was observed (Figure 2D, lanes 7-10). Taken together, these data show that the novel *SF3B1* in-frame deletions p.K700del and p.Q698del use intronic features to induce aberrant splicing identical to the most frequent hotspot mutant p.K700E.

To examine the sensitivity of these novel *SF3B1* deletions to pharmacologic splicing modulation in comparison with p.K700E, we used the splicing modulator E7107 known to cross-link the SF3b complex.[21] An MTS assay on primary leukemia cells from CLL patients after treatment with E7107 showed a dose response similar to $SF3B1^{K700E}$ and $SF3B1^{WT}$ cells (IC_{50} of ~4-10 nM; Figure 2E). This suggests that *SF3B1* deletions discovered in this study may be therapeutically sensitive targets for splicing modulators. Indeed, an orally available SF3B1 modulator is currently being evaluated in phase 1 clinical trials (www.clinicaltrials.gov; #NCT02841540).

Here we report the identification, characterization, and sensitivity to splicing modulation of 2 novel *SF3B1* in-frame deletions found in CLL. The colocalization of p.K700E hotspot mutation and these novel deletions highlight the functional importance of this region in *SF3B1*. These findings for *SF3B1* are analogous to functionally similar oncogenic in-frame deletions that have been described surrounding

Figure 1. (continued) linear correlation between mutation allele frequency (%) and ss usage (PSI). Colors for splicing markers: light green, *MAP3K7*; light blue, *DYNLL1*; gray, *TMEM14C*; purple, *ZDHHC16*. Shapes for *SF3B1* mutation status: circle, WT; triangle, p.K700E; square, p.K700del; star, p.Q698del. (E) Homology model based on cryo-electron microscopy structure of Hsh155 (SF3B1 homolog in yeast) interacting with pre–messenger RNA (pre-mRNA) near the deletion site (K700 and Q698 represented as magenta spheres, PDB: 5GM6) and crystal structure of apo-SF3B1 (PDB: 5IFE) are shown in top panel. Homology modeling of SF3B1 in-frame deletions, K700del and Q698del, based on the crystal structure (PDB: 5IFE) are shown in the bottom panel. The affected amino acid side chains are represented in stick (magenta), rest of the protein (yellow), and pre-mRNA (gray) in illustration.

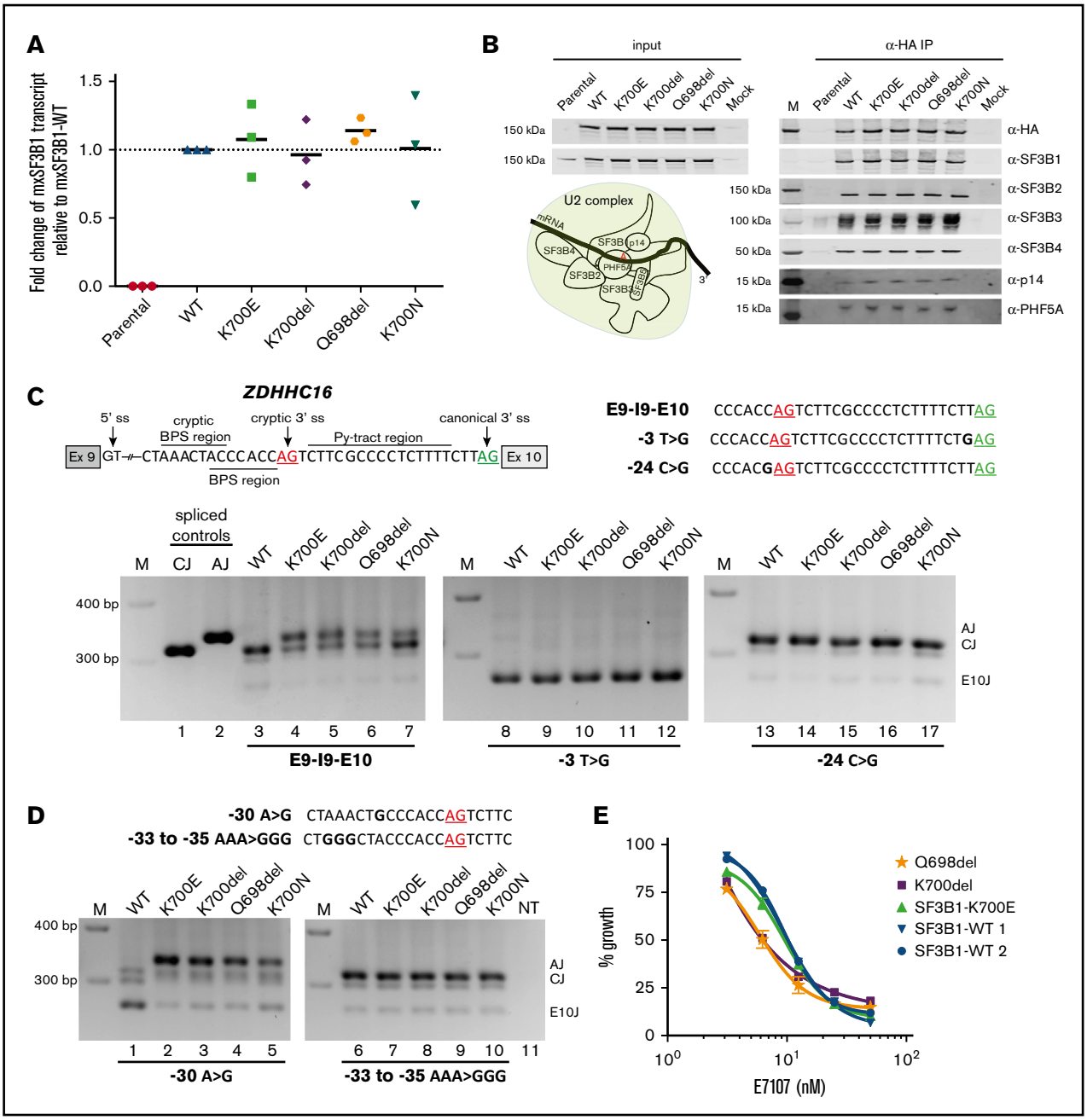

Figure 2. Expression and functional characterization of *SF3B1* in-frame deletions. (A) Fold change of mxSF3B1 variant transcript relative to WT (calculated as $2^{-\Delta\Delta CT}$) in HEK293FT cells transfected with mxSF3B1 WT, K700E, K700del, Q698del, and K700N complementary DNA constructs. Data are represented as mean ± standard error of the mean, n = 3. (B) Incorporation of SF3B1 variants in SF3b complex is shown through western blot analysis of 5 different complex partners after coimmunoprecipitation using α-HA beads. Input cell lysates are shown in the left panel, and the eluted IP samples are shown in the right panel. Schematic of SF3b in U2 complex is also shown with pre-mRNA branch site labeled as "A." (C-D) Schematic of *ZDHHC16* minigene labeled with ss's is shown with cryptic AG (red) and canonical AG (green) underlined. Total RNA isolated from HEK293FT cotransfection of mxSF3B1 variants (WT, K700E, K700del, Q698del, K700N) with any of the 3 different *ZDHHC16* minigenes (E9-I9-E10, −3T>G, −24C>G) (C) or with any of the 2 different *ZDHHC16* minigenes (−30A>G, −33 to −35 AAA>GGG) (D) was used for reverse transcription PCR and visualized by ethidium-bromide stained 2.5% agarose gel. Sequences of different minigenes with specific mutations highlighted in bold are shown for respective gels. Spliced controls of canonical (CJ) and aberrant junction (AJ) are in lanes 1 and 2, marker is denoted as M, and nontransfected control is shown as NT. Spliced product for junction in exon 10 is shown as E10J. (E) Effects of splicing inhibitor E7107 treatment on viability of primary CLL patient cells (K700del, Q698del, SF3B1-K700E, SF3B1-WT 1, and SF3B1-WT 2) measured through MTS assay. E7107 concentration is plotted in log scale in the x-axis; % absorbance in the colorimetric assay is represented as % growth in the y-axis. Data are represented as mean ± standard deviation, n = 3.

hotspot mutations in the splicing factor *SRSF2*,[3] and several oncogenes such as *CTNNB1* and *NFE2L2*, encoding oncoproteins β-catenin and NRF2, respectively.[22-25] Although the novel SF3B1 deletions we report here could compromise the superhelical flexibility and constitutively force an alternative conformation inducing changes in the protein-RNA interactome, they still induce aberrant splicing and maintain sensitivity toward splicing modulation, thus rendering them as therapeutic targets for treating spliceosome-mutant cancers.

Acknowledgments

The authors are grateful to patients and families for participating in clinical trials and providing samples; the authors also thank H3 Biomedicine employees for their support in this project.

This work was supported in part by grants from the Alliance Foundation for Clinical Trials in Oncology (J.S.B.) and the National Institutes of Health, National Cancer Institute (grants K23 CA178183 [J.A.W.] and R35 CA197734-01 [J.C.B.]).

Authorship

Contribution: M.S. and L.Y. conducted the bioinformatics analyses of RNA-seq data; A.A.A. performed the structure modeling, qPCR, immunoblotting, and minigene assays; R.M. prepared sequencing experiments; L.T.B. performed viability assays; J.S.B. and R.L. collected and analyzed viability experiment in patient samples; A.J.J., J.A.W., and J.C.B. provided reagents and patient samples; M.W., P.G.S., A.A.A., M.S., L.Y., J.S.B., and S.B. guided the experiments; A.A.A., M.S., J.S.B., and S.B. wrote the manuscript; and all authors reviewed and approved the final manuscript.

Conflict-of-interest disclosure: A.A.A., M.S., M.W., P.Z., L.Y., P.G.S., and S.B. are full time employees of H3 Biomedicine, Inc. The remaining authors declare no competing financial interests.

Correspondence: Silvia Buonamici, H3 Biomedicine, Inc., 300 Technology Sq, Cambridge, MA 02139; e-mail: silvia_buonamici@h3biomedicine.com.

References

1. Papaemmanuil E, Cazzola M, Boultwood J, et al; Chronic Myeloid Disorders Working Group of the International Cancer Genome Consortium. Somatic SF3B1 mutation in myelodysplasia with ring sideroblasts. *N Engl J Med*. 2011;365(15):1384-1395.
2. Wang L, Lawrence MS, Wan Y, et al. SF3B1 and other novel cancer genes in chronic lymphocytic leukemia. *N Engl J Med*. 2011;365(26):2497-2506.
3. Yoshida K, Sanada M, Shiraishi Y, et al. Frequent pathway mutations of splicing machinery in myelodysplasia. *Nature*. 2011;478(7367):64-69.
4. Yoshida K, Ogawa S. Splicing factor mutations and cancer. *Wiley Interdiscip Rev RNA*. 2014;5(4):445-459.
5. Papasaikas P, Valcárcel J. The spliceosome: the ultimate RNA chaperone and sculptor [published correction appears in *Trends Biochem Sci*. 2016;41(4):386]. *Trends Biochem Sci*. 2016;41(1):33-45.
6. Yan C, Wan R, Bai R, Huang G, Shi Y. Structure of a yeast activated spliceosome at 3.5 Å resolution. *Science*. 2016;353(6302):904-911.
7. Cretu C, Schmitzová J, Ponce-Salvatierra A, et al. Molecular architecture of SF3b and structural consequences of its cancer-related mutations. *Mol Cell*. 2016;64(2):307-319.
8. Rauhut R, Fabrizio P, Dybkov O, et al. Molecular architecture of the Saccharomyces cerevisiae activated spliceosome. *Science*. 2016;353(6306):1399-1405.
9. Darman RB, Seiler M, Agrawal AA, et al. Cancer-associated SF3B1 hotspot mutations induce cryptic 3′ splice site selection through use of a different branch point. *Cell Reports*. 2015;13(5):1033-1045.
10. Alsafadi S, Houy A, Battistella A, et al. Cancer-associated SF3B1 mutations affect alternative splicing by promoting alternative branchpoint usage. *Nat Commun*. 2016;7:10615.
11. Tang Q, Rodriguez-Santiago S, Wang J, et al. SF3B1/Hsh155 HEAT motif mutations affect interaction with the spliceosomal ATPase Prp5, resulting in altered branch site selectivity in pre-mRNA splicing. *Genes Dev*. 2016;30(24):2710-2723.
12. Carrocci TJ, Zoerner DM, Paulson JC, Hoskins AA. SF3b1 mutations associated with myelodysplastic syndromes alter the fidelity of branchsite selection in yeast. *Nucleic Acids Res*. 2017;45(8):4837-4852.
13. Kesarwani AK, Ramirez O, Gupta AK, et al. Cancer-associated SF3B1 mutants recognize otherwise inaccessible cryptic 3′ splice sites within RNA secondary structures. *Oncogene*. 2017;36(8):1123-1133.
14. Visconte V, Makishima H, Jankowska A, et al. SF3B1, a splicing factor is frequently mutated in refractory anemia with ring sideroblasts. *Leukemia*. 2012;26(3):542-545.
15. Makishima H, Visconte V, Sakaguchi H, et al. Mutations in the spliceosome machinery, a novel and ubiquitous pathway in leukemogenesis. *Blood*. 2012;119(14):3203-3210.
16. Rossi D, Bruscaggin A, Spina V, et al. Mutations of the SF3B1 splicing factor in chronic lymphocytic leukemia: association with progression and fludarabine-refractoriness. *Blood*. 2011;118(26):6904-6908.
17. Messina M, Del Giudice I, Khiabanian H, et al. Genetic lesions associated with chronic lymphocytic leukemia chemo-refractoriness. *Blood*. 2014;123(15):2378-2388.
18. DeBoever C, Ghia EM, Shepard PJ, et al. Transcriptome sequencing reveals potential mechanism of cryptic 3′ splice site selection in SF3B1-mutated cancers. *PLOS Comput Biol*. 2015;11(3):e1004105.
19. Conte S, Katayama S, Vesterlund L, et al. Aberrant splicing of genes involved in haemoglobin synthesis and impaired terminal erythroid maturation in SF3B1 mutated refractory anaemia with ring sideroblasts. *Br J Haematol*. 2015;171(4):478-490.

20. Ilagan JO, Ramakrishnan A, Hayes B, et al. U2AF1 mutations alter splice site recognition in hematological malignancies. *Genome Res*. 2015;25(1):14-26.

21. Kotake Y, Sagane K, Owa T, et al. Splicing factor SF3b as a target of the antitumor natural product pladienolide. *Nat Chem Biol*. 2007;3(9):570-575.

22. Takayasu H, Horie H, Hiyama E, et al. Frequent deletions and mutations of the beta-catenin gene are associated with overexpression of cyclin D1 and fibronectin and poorly differentiated histology in childhood hepatoblastoma. *Clin Cancer Res*. 2001;7(4):901-908.

23. Ahn SM, Jang SJ, Shim JH, et al. Genomic portrait of resectable hepatocellular carcinomas: implications of RB1 and FGF19 aberrations for patient stratification. *Hepatology*. 2014;60(6):1972-1982.

24. Pilati C, Letouzé E, Nault JC, et al. Genomic profiling of hepatocellular adenomas reveals recurrent FRK-activating mutations and the mechanisms of malignant transformation. *Cancer Cell*. 2014;25(4):428-441.

25. Campbell JD, Alexandrov A, Kim J, et al; Cancer Genome Atlas Research Network. Distinct patterns of somatic genome alterations in lung adenocarcinomas and squamous cell carcinomas. *Nat Genet*. 2016;48(6):607-616.